第 30 卷第 4 期
2014 年 4 月

无 机 化 学 学 报
CHINESE JOURNAL OF INORGANIC CHEMISTRY

Vol.30 No.4
961-968

Fe^{3+}掺杂三维分级纳米 Bi_2WO_6 的合成及其光催化活性增强机理

王丹军*,[1,2] 岳林林[1] 郭 莉[1] 张 洁[1] 付 峰*,[1] 薛岗林[2]

([1]延安大学化学与化工学院,陕西省化学反应工程重点实验室,延安 716000)

([2]教育部合成与天然产物重点实验室,西北大学化学系,西安 710069)

摘要: 利用水热法合成了 Fe^{3+}掺杂的三维分级纳米 Bi_2WO_6, 借助 X 射线衍射 (XRD)、场发射扫描电镜 (FE-SEM)、透射电镜 (HRTEM)、能谱(EDS)、紫外可见漫反射(UV-Vis-DRS)等测试手段对所得样品的相组成、形貌和谱学特征进行了表征。选择罗丹明 B 为模型污染物研究所得样品在可见光下的催化活性。结果表明,Fe^{3+}掺杂 Bi_2WO_6 为新颖的分级纳米结构,且 Fe^{3+}掺杂能有效提高 Bi_2WO_6 的光催化活性,Fe^{3+}掺杂量对 Bi_2WO_6 活性的影响显著;实验结果还表明,所得 Fe^{3+}掺杂 Bi_2WO_6 催化剂的稳定性较好,易于回收。此外,还对 Fe^{3+}掺杂 Bi_2WO_6 的光催化活性增强机理进行了研究,缺电子的 Fe^{3+}作为电子捕获中心有利于促进光生电子–空穴对的分离,从而提高 Bi_2WO_6 的光催化活性。

关键词: 光催化; 三维分级 Bi_2WO_6; Fe^{3+}掺杂; 活性增强机理

中图分类号: O643.36 **文献标识码**: A **文章编号**: 1001-4861(2014)04-0961-08

DOI: 10.11862/CJIC.2014.137

Synthesis and Enhanced Photocatalytic Mechanism of Fe^{3+} Doped Three-Dimensional Bi_2WO_6 Hierarchical Nanoarchitectures

WANG Dan-Jun*,[1,2] YUE Lin-Lin[1] GUO Li[1] ZHANG Jie[1] FU Feng*,[1] XUE Gang-Lin[2]

([1]*College of Chemistry &Chemical Engineering, Yan'an University, Shaanxi Key Laboratory of Chemical Reaction Engineering, Yan'an, Shaanxi* 716000, *China*)

([2]*Key Laboratory of Synthetic and Natural Functional Molecule Chemistry, Department of Chemistry, Northwest University, Xi'an* 710069, *China*)

Abstract: Fe^{3+} doped three-dimensional Bi_2WO_6 hierarchical nanoarchitectures have been synthesized via a hydrothermal process. XRD, FE-SEM, HRTEM, EDS and UV-Vis-DRS techniques were employed to characterize the phase composition, morphology and spectrum properties of the as-synthesized samples. Rhodamine B was selected as a model pollutant to investigate the photocatalytic activity of the as-synthesized sample under visible-light. The results indicate that Fe^{3+} doped Bi_2WO_6 exhibits a novel hierarchical nanoarchitectures, and Fe^{3+} doping can enhance the photocatalytic activity of Bi_2WO_6 photocatalyst, the amount of Fe^{3+} doping has a serious effect on the photocatalytic activity of Bi_2WO_6 photocatalyst. The results also reveal that Fe^{3+} doped Bi_2WO_6 nanoarchitecture with high stability is easy to be recycled. Furthermore, the mechanism for the enhancement of the photocatalytic activity was also investigated. The doped electron deficient Fe^{3+} ions could act as electron traps and facilitate the separation of photogenerated electron-hole pairs, thus improve the photocatalytic efficiency.

Key words: photocatalysis; 3D hierarchical Bi_2WO_6; Fe^{3+} doping; photocatalytic activity enhancement mechanism

收稿日期:2013-10-11。收修改稿日期:2013-12-05。

国家自然科学基金(No.20973133,21073106);陕西省科技厅工业攻关项目(No.2013K11-08);陕西省科技厅统筹项目(No.2012KG03-16)陕西省教育厅科研基金(No.13JK0669);陕西省化学反应工程重点实验室专项科研基金(No.12JS117);延安市工业攻关项目(No.2011kg-13),延安大学重点项目(No.YD22013-07)资助。

*通讯联系人。E-mail:wangdj761118@163.com

0 Introduction

As advanced oxidation technology, heterogeneous photocatalysis has been received considerable attention on the water treatment to remove toxicants. Titanium dioxide (TiO_2) has been extensively studied because of its high activity, long-term stability, low price and availability[1-2]. However, TiO_2 can only absorb the ultraviolet light, which constitutes 3%~5% of solar light due to its relatively inefficient quantum yield and the wide band gap. In order to make better use of solar light energy it is vital to develop photocatalytic materials which are visible light active. Bi-based photocatalysts, including Bi_2WO_6, might be excited by visible light and display potential photocatalytic efficiency to many organic contaminant degradation and water splitting[3-8]. However, their application is still limited due to the high electron-hole recombination rate in the process of photocatalytic reaction.

Generally speaking, it is a useful method to extend the photoresponse region of photocatalysts by doping a certain amount of metal or nonmetal elements to improve the migration efficiency of photo-generated electrons and suppress the recombination of electrons and holes effectively. At present, noble metals[9], transition metals[10] and nonmetal elements[11-13] have been doped in Bi_2WO_6 and the composite photocatalysts display high efficiency to pollutants under visible light irradiation. Up to date, although many effects have been made to improve the activity of Bi_2WO_6 photocatalysts, there are still some drawbacks hindering their lifetimes and the limited region of visible-light photo-response. To meet the requirements of future practical performance of Bi_2WO_6 photocatalysts, it is still necessary to design novel Bi_2WO_6-based photocatalysts to further improve their photocatalytic efficiencies.

Very recently, our group has synthesized 3D mesoporous Bi_2WO_6 nanostructure by a facile hydrothermal method without any additives[14]. Furthermore, Ag nanoparticles were deposited on the surface of Bi_2WO_6 via a following facile photoreduction process. The photocatalysis results revealed that Ag-loaded Bi_2WO_6 exhibited high photocatalytic activity compared with pure Bi_2WO_6[15]. The aim of this work is to dope Bi_2WO_6 with Fe^{3+} and investigate the Fe^{3+} doping effect on the photocatalytic activity of Bi_2WO_6. Fe^{3+} doped Bi_2WO_6 hierarchical nanoarchitecture has been synthesized via a facile hydrothermal process and characterized by XRD, FE-SEM, EDS, UV-Vis-DRS. In addition, the photocatalytic activity enhancement mechanism of Bi_2WO_6 hierarchical nanoarchitecture is also discussed in this article.

1 Experimental

1.1 Synthesis and characterization

All chemicals were analytical grade and used without further purification. In a typical process[14], for synthesizing pure Bi_2WO_6 nanoarchitectures, 1.0 mmol $Bi(NO_3)_3$ was first dissolved in 20 mL of nitric solution (0.4 mol·L^{-1}), and a desired amount of $Fe(NO_3)_3$ at 0.1 mol·L^{-1} was added into the solution of $Bi(NO_3)_3$, resulting in the molar ratio of Fe to Bi as 0.5%, 1.0%, 2.0%, and 5.0%. Then, 10 mL of $(NH_4)_{10}W_{12}O_{41}$ solution with concentration of 0.008 2 mol·L^{-1} was added dropwisely to the above solution under vigorous magnetic stirring. After being magnetic stirred for 2 h, the resulting precursor suspension was transferred into a 50 mL Teflon-lined autoclave and then sealed and maintained at 190 ℃ for 4 h. Subsequently, the autoclave was cooled to room temperature naturally. After filtration, the yellowish white precipitate was collected and washed with distilled water, and absolute ethanol several times, then dried under vacuum at 80 ℃ for 4 h. The resulted samples were denoted as 0.5%, 1.0%, 2.0%, and 5.0% Fe/Bi_2WO_6, respectively.

The purity and crystalline structure of the samples were characterized with a Shimadzu XRD-7000 X-ray diffractometer (XRD) with Cu $K\alpha$ radiation (λ =0.154 18 nm). The accelerating voltage and the applied current were 40 kV and 30 mA, respectively. The morphology of the sample was observed by the field emission scanning electron microscope (FE-SEM, JSM-6700F). The pore diameter distribution and surface area of Bi_2WO_6 architectures were measured

by nitrogen adsorption/ desorption (Automated Physisorption and Chemisorption Analyser, Micromeritics ASAP 2010).

1.2 Photocatalytic activity

The evaluation of photocatalytic performance of samples for photocatalytic decolorization of Rhodamin B (RhB) aqueous solution was performed as follows: A 500 W Xe-arc lamp was used as the visible-light source with a cutoff filter to cut off the light below 450 nm. The suspensions containing 200 mg of photocatalyst and 250 mL fresh aqueous solution of RhB (10 mg·L^{-1}) were continuously magnetically stirred in the dark for 0.5 h to establish an adsorption/ desorption equilibrium of RhB solution. Then, the light source was turned on. During the reaction, 5 mL of samples were taken at given time intervals and then separated from Bi_2WO_6 photocatalyst through centrifugation. The supernatant solution was decanted and the absorbance of RhB at 553 nm was monitored.

2 Results and discussion

2.1 XRD characterization

The lattice parameters, crystallite size and BET specific surface area are summarized in Table 1. The XRD patterns are compared in Fig.1, and the diffraction peaks can be categorized into different sets: the peaks at 2θ of 28.3°, 32.8°, 32.9°, 47.0°, 47.1°, 55.8°, 58.5°, 68.7°, 75.9° and 78.5° can be perfectly indexed to orthorhombic Bi_2WO_6 (PDF No. 39-0256), corresponding to the indices of (131), (200), (002) , (260), (202), (331), (262), (400), (103) and (204) planes, respectively (Fig.1a ~e). No peaks of impurities are detected, indicating satisfactory purity of the products. After refinement, the lattice parameters of the samples are obtained (Table 1). It is

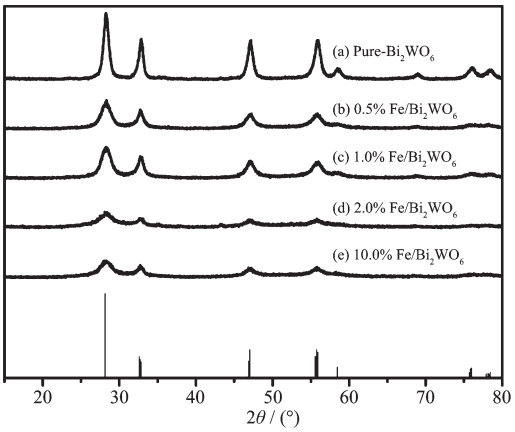

Fig.1　XRD patterns of as-prepared samples

clear that there is an obvious change in lattice parameters between Bi_2WO_6. Lattice distortion of Fe^{3+} doped Bi_2WO_6 may be attributed to two reasons. On one hand, Fe^{3+} doping may replace the Bi^{3+} of $Bi_2O_2^{2+}$ layer, which may cause the lattice parameters decreasing. On the other hand, 3*d* orbitals of Fe^{3+} repulsion may lead to increasing cell parameters. Integration these two factors, Fe^{3+} doping causes the lattice parameters of Bi_2WO_6 to exhibit a first increase and then decrease, and the lattice parameter distortion is more obvious when doped amount of Fe^{3+} is more than 2.0%. In the experimental results, the cell volume reduction ratio reaches 3.02% with 10.0% Fe^{3+} doping. In addition, we can see that the XRD patterns of pure-Bi_2WO_6 and Fe^{3+} doped Bi_2WO_6 products show sharp peaks with high intensity. It indicates that the as-obtained Bi_2WO_6 sample has high crystallinity. This is beneficial to photocatalysis because high crystallinity generally means fewer traps and stronger photocatalytic activity[15].

2.2 Morphology and porous structure

The morphologies and microstructures of pure-Bi_2WO_6 and Fe^{3+} doped Bi_2WO_6 samples are shown in

Table 1　Cell parameters and crystallite size of as-prepared photocatalysts

Sample	Cell parameters			Cell volume	S_{BET} / ($m^2 \cdot g^{-1}$)
	a / nm	*b* / nm	*c* / nm	*V* / nm^3	
Pure-Bi_2WO_6	0.544 03	1.639 05	0.543 62	0.484 75	24
0.5% at-Bi_2WO_6	0.545 68	1.643 55	0.543 82	0.487 73	26
1.0% at-Bi_2WO_6	0.545 80	1.643 44	0.543 48	0.487 74	26
2.0% at-Bi_2WO_6	0.542 16	1.654 43	0.544 47	0.488 37	32
10.0% at-Bi_2WO_6	0.545 54	1.640 48	0.543 29	0.486 22	31

Fig.2 ~3. It can be clearly seen that pure-Bi_2WO_6 exhibits hierarchical spherical architecture of 2~3 μm and Fe^{3+} doped Bi_2WO_6 samples show the same morphology (Fig.2b ~2d). Interestingly, the spherical Bi_2WO_6 hierarchical architectures have many small secondary nanoplates. Further information about the pure-Bi_2WO_6 architectures from FE-SEM images is shown in insets of Fig.2a and Fig.3b. From these figures, it can be seen that the spherical Bi_2WO_6 nanoarchitectures are built up by nanoplates with diameters of 10~20 nm, and the size does not exhibit obvious change with doping of Fe^{3+} (Fig.2c ~2d and Fig.3c ~d). The single crystalline nature and parameters of nanoplates by HR-TEM is given in inset of Fig.2b. Fig.3f is the enlarged TEM image of the area marked by a red circle in Fig.3b. Obviously, the nanoplates can be seen, which assemble into one layer with their sides. The SAED (selected area electron diffraction) pattern (inset in Fig.3b) exhibits a regular and clear diffraction spot array and can be indexed to single crystalline Bi_2WO_6. From the High-resolution TEM (HR-TEM) shown in Fig.3d (inset in right corner), the lattice interplanar spacing is 0.315 nm, corresponding to the (131) plane of orthorhombic Bi_2WO_6 and is well consistent with the XRD pattern in Fig.1. This result also confirms the single structure of the nanoplates. In comparsion, Fe^{3+} doping does not change the morphology and size of Bi_2WO_6 hierarchical architectures (Fig.2~3). For comparison of the HR-TEM of pure-Bi_2WO_6 and Fe^{3+} doping Bi_2WO_6 (Fig.3b and Fig.3d), lattice interplanar spacing is 0.315 nm and 0.321 nm, corresponding to the (131) planes of orthorhombic pure-Bi_2WO_6 and 2.0% Fe^{3+} doping Bi_2WO_6, respectively. According to the literature [14], it is the surface electrostatic effect that causes the Bi_2WO_6 nanoplates to be assembled into the novel three-dimensional structure. With Fe^{3+} doping into the lattice of Bi_2WO_6, the charge distribution of nanoplate changes, which causes the size of Bi_2WO_6 architectures decreasing and the surface area increasing. Further evidence for the chemical composition of the as-prepared 2.0% Fe/Bi_2WO_6 architectures was obtained by EDS technique. It can be seen that the sample contains only Bi, W, O and Fe elements (Fig.2e). Furthermore, the quantitative analysis reveals that the atomic ratio of Bi:W:O:Fe in 2.0% Fe/Bi_2WO_6 is 2:1:6.02:0.019, which is consistent with the theoretical value.

The BET surface areas for pure-Bi_2WO_6, 0.5% Fe/Bi_2WO_6, 1.0% Fe/Bi_2WO_6, 2.0% Fe/Bi_2WO_6 and

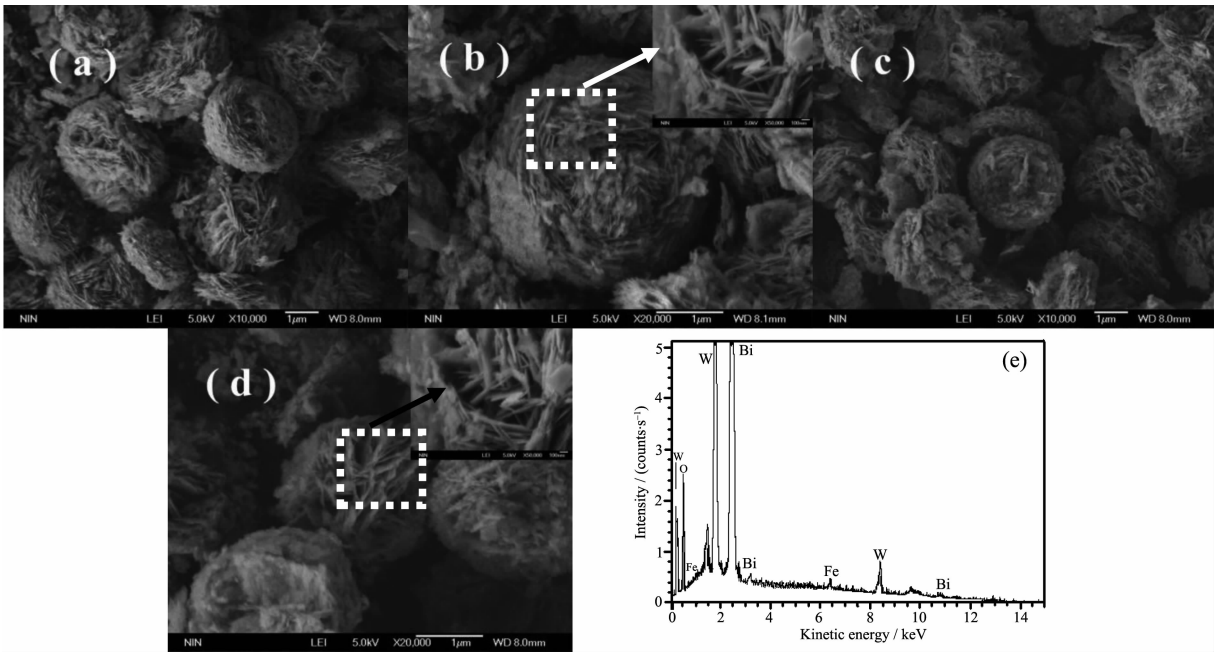

(a~b) Pure-Bi_2WO_6; (c~d) 2.0% Fe^{3+} doped Bi_2WO_6; (e) EDS spectrum of 2.0% Fe/Bi_2WO_6

Fig.2 SEM images and EDS spectrum of samples

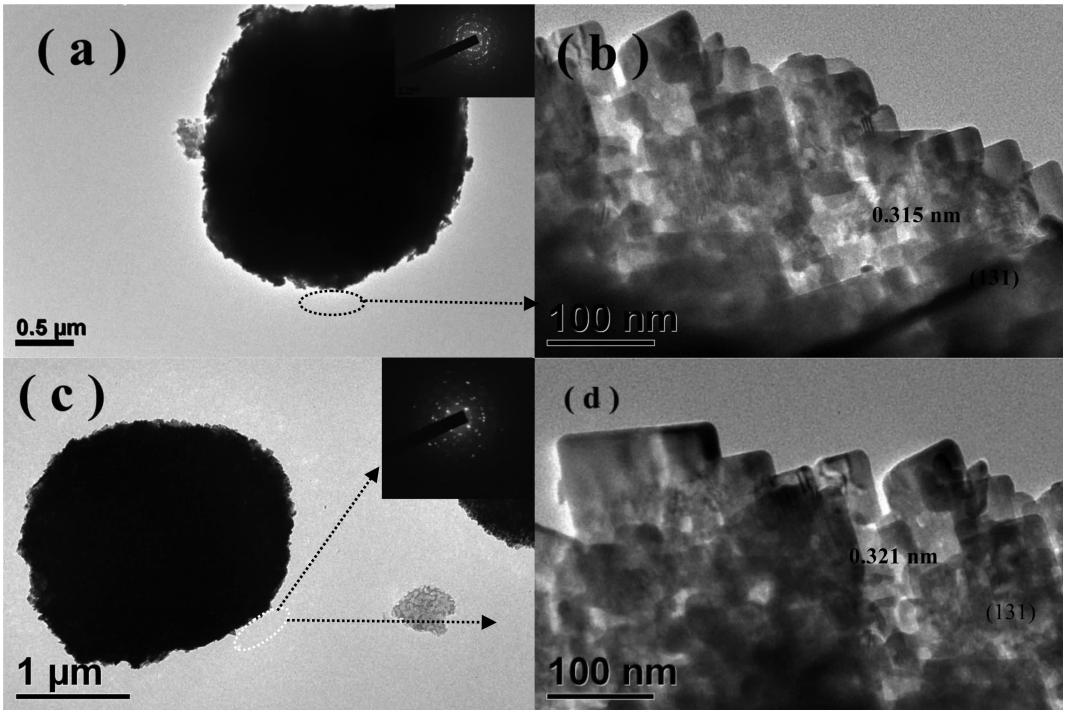

(a~b) Pure-Bi_2WO_6: (a) TEM image and its corresponding SAED of an individual Bi_2WO_6 hierarchical nanoarchitecture, (b) Enlarged TEM and HRTEM image and SAED of a simple nanoplate showing its single-crystal nature; (c~d) 2.0% Fe^{3+} doped Bi_2WO_6: (c) TEM image and SAED of an individual 2.0% Fe^{3+} doped Bi_2WO_6 hierarchical nanoarchitecture, and Enlarged TEM, HRTEM image and SAED of a simple nanoplate

Fig.3　TEM and HRREM image of pure- Bi_2WO_6 and 2.0%Fe^{3+} doped Bi_2WO_6

10.0% Fe/Bi_2WO_6 are 24, 26, 26, 32 and 31 $m^2 \cdot g^{-1}$, respectively. The largest surface area of 32 $m^2 \cdot g^{-1}$ is achieved when the doping amount of Fe^{3+} reaches 2.0%. Increasing the doping amount of Fe^{3+} to 10%, BET surface area of the products have no obvious change, the value is 31 $m^2 \cdot g^{-1}$ (Table 1).

2.3　Optical absorption properties

The typical UV-Vis diffuse reflection spectra (UV-Vis-DRS) of Fe^{3+} doped Bi_2WO_6 is compared with that of pure-Bi_2WO_6 in Fig.4. Pure-Bi_2WO_6 presents the photoabsorption properties from the UV light region to visible light about 450 nm due to the intrinsic band gap transition. The absorption spectra of Fe^{3+} doped Bi_2WO_6 is obviously different from that of pure Bi_2WO_6. The adsorption edge shows a "red-shift" comparison to that of pure-Bi_2WO_6. The band gap was calculated with the formula of E_g=1 024/λ_g, where E_g and λ_g represent band gap and absorption edge, respectively. The band gap energies estimated from the intercept of the tangents to the plots are 2.95, 2.85, 2.82 and 2.72 eV for samples of pure Bi_2WO_6, 0.5% Fe^{3+} doped Bi_2WO_6, 1.0% Fe^{3+} doped Bi_2WO_6, 2.0%Fe^{3+} doped Bi_2WO_6 and 10.0% Fe^{3+} doped Bi_2WO_6, respectively.

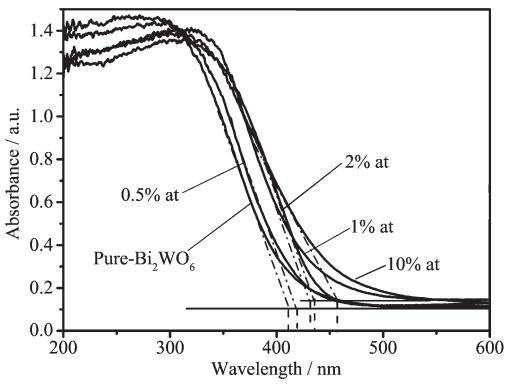

Fig.4　UV-Vis DRS spectra of pure-Bi_2WO_6 and Fe^{3+} doped Bi_2WO_6 samples

2.4　Photocatalytic activities enhancement mechanism of Fe^{3+} doped Bi_2WO_6

The photocatalytic performances for the degradation efficiency of RhB by the Fe^{3+} doped Bi_2WO_6 with different Fe contents are given in Fig.5. In the control test, less than 5% of RhB is degraded in 50

min. When a 500 W Xe-arc lamp is used as the visible light source (with a cutoff filter to cut off the light below 420 nm), as-prepared Fe^{3+} doped Bi_2WO_6 shows a better photocatalytic activity for RhB degradation than that of pure-Bi_2WO_6. After being irradiated for 50 min, about 75%, 80%, 85%, 98% and 80% of RhB is degraded by pure Bi_2WO_6, 0.5% Fe/Bi_2WO_6, 1.0% Fe/Bi_2WO_6, 2.0% Fe/Bi_2WO_6 and 10.0% Fe/Bi_2WO_6, respectively. As the doping amount of Fe^{3+} increases to 2.0%, the photocatalytic activity of Fe/Bi_2WO_6 displays the highest degradation efficient. About 98% RhB could be removed in 50 min.

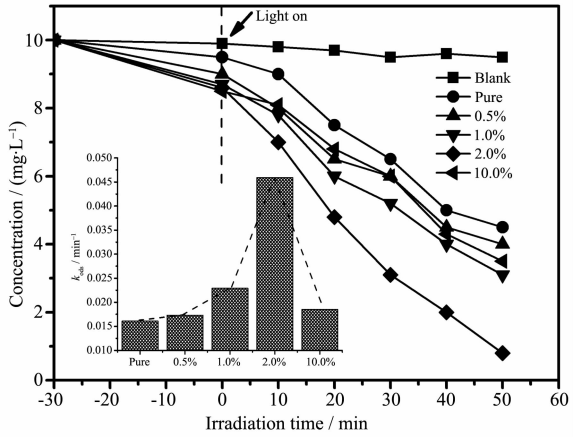

Fig.5 Photocatalytic activity of pure-Bi_2WO_6 and Fe^{3+} doped Bi_2WO_6 samples

The degradation kinetics follows a pseudo first-order kinetic model: $\ln(c/c_0)=k_{obs}t$ where k_{obs}, c and c_0 represent the pseudo first-order degradation rate constant, the concentration of RhB at reaction time t and the beginning of the reaction. The k_{obs} is determined by plotting $\ln(c/c_0)$ versus reaction time t and it gives an indication of photocatalytic activity of the photocatalyst. The k_{obs} value are given in the inset of Fig.5. Apparently, k value of 2.0% Fe/Bi_2WO_6 nanoarchitecture is higher than others, and is nearly three times as fast as that of pure Bi_2WO_6, which is in accord with the curves of the catalysts′ photocatalytic activities. The high photocatalytic degradation efficiency of Fe doping Bi_2WO_6 nanoarchitecture could be explained in two aspects: firstly, the relatively large surface area of as-synthesized sample favors the adsorption of RhB. As shown in Fig.5, about 5% of RhB is adsorbed on pure-Bi_2WO_6. However, the adsorption on 0.5%, 1.0%, 2.0%, and 10.0% Fe/Bi_2WO_6 increases to around 12.5%. Secondly, as a typical Lewis acid, the doped Fe^{3+} is electron deficient, which could act as electron traps and facilitate the separation of photogenerated electron-hole pairs, thus improve the photocatalytic efficiency. When the doping amount of Fe^{3+} increases to 10%, the photoactivity decreases and is similar to pure-Bi_2WO_6. It was reported that excessive metal elements could become recombination centers of electron and hole, leading to lower photocatalytic efficiency[16].

The photogenerated ·OH radicals and photogenerated hole are primary oxidative species in a photocatalytic decoloration reaction [17-19]. In order to ascertain the active species responsible for the photocatalytic degradation process, isopropanol as a radical scavenger and KI as a hole scavenger were added into the solution. As shown in Fig.6, the degradation efficiency is not affected significantly by adding isopropanol, suggesting that ·OH is not the main reactive species responsible for the degradation of RhB by 2.0% Fe^{3+}/Bi_2WO_6. According to the literature[20-21], ·OH could not be produced for the pure-Bi_2WO_6 due to the more negative redox potential of Bi^{V}/Bi^{III} (+1.59 eV) than that of ·OH/OH^- (+1.99 eV) and OH/H_2O (2.27 eV). While doping Fe^{3+} in Bi_2WO_6 does not change the valence band significantly, it is expected that ·OH is not produced in the system with 2.0% Fe^{3+}/Bi_2WO_6. However, the reaction is suppressed as 0.15 mol·L^{-1} KI is added to the reaction solution,

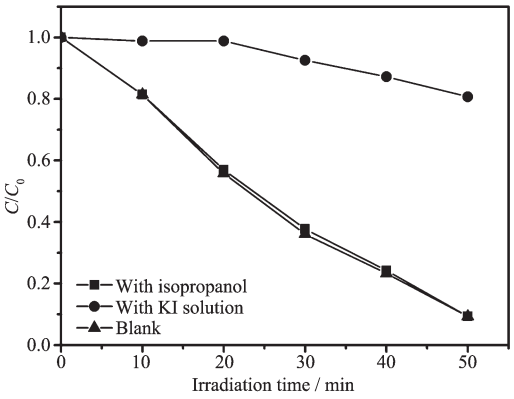

Fig.6 Effect of isopropanol and KI on the photocatalytic activity of Fe^{3+} doped Bi_2WO_6 sample under simulated sunlight irradiation

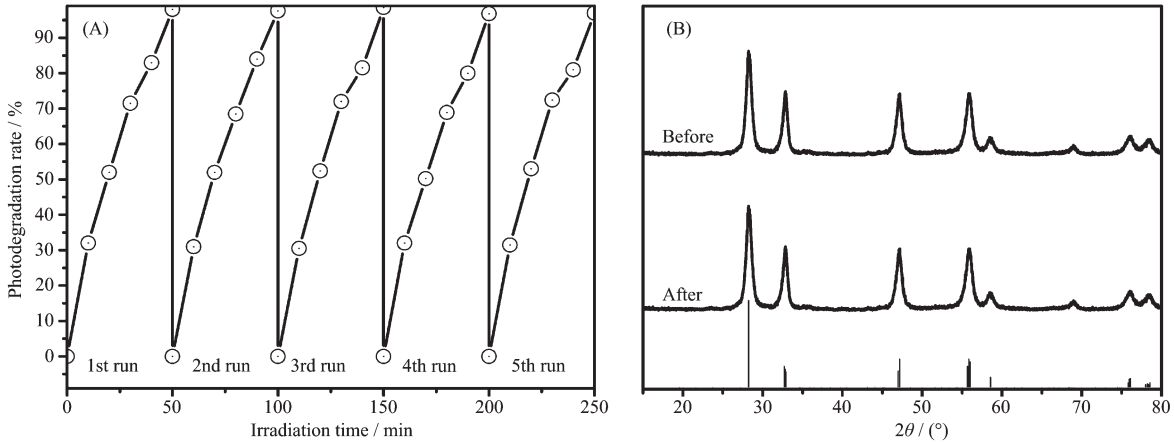

Fig.7　Recycling of photocatalytic degradation of RhB on the 2.0% Fe^{3+}/Bi_2WO_6 nanoarchitecture under simulated sunlight irradiation (A) and comparison of XRD pattern of 2.0% Fe^{3+}/Bi_2WO_6 before and after use (B)

indicating that photogenerated hole is responsible for the degradation. As the Fe^{3+} is electron deficient, it could trap electron and promote the separation of electron and hole. When the photocatalyst is irradiated, the photogenerated hole (h^+) might attack RhB molecules directly and cause RhB decomposition.

To demonstrate the potential applicability of Fe^{3+} doped Bi_2WO_6 photocatalysts, the stability of as-prepared 2.0% Fe^{3+}-Bi_2WO_6 spherical nanoarchitecture was investigated. Experimental results show that 2.0% Fe^{3+} doped Bi_2WO_6 nanoarchitecture exhibits significantly enhanced photocatalytic activity in photodegradation of RhB, and has high stability and is easy to be recycled (Fig.7A). After five recycles, the catalyst exhibits no obvious loss of activity. Fig.7B shows the XRD patterns of 2.0% Fe^{3+}-Bi_2WO_6 photocatalyst before and after use. It is found that there is no change in position and intensity of all diffraction peaks and there is no other phases detected.

3　Conclusions

Fe^{3+} doping Bi_2WO_6 photocatalyst was synthesized via a hydrothermal process using $Fe(NO_3)_3$, $(NH_4)_{10}W_{12}O_{41}$ and Bi $(NO_3)_3\cdot 5H_2O$ as starting materials. The results indicate that Fe^{3+} doping leads to the adsorption edge of Bi_2WO_6 showing a "red-shift" compared to that of pure-Bi_2WO_6. On the other hand, Fe^{3+} doping can enlarge the surface area of Bi_2WO_6. As the result, Fe^{3+} doping improves the photocatalytic activity of Bi_2WO_6 photocatalyst. In addition, the doping amount of Fe^{3+} has a serious effect on the photocatalytic activity of Bi_2WO_6 photocatalyst. When the doping amount of Fe^{3+} increases to 2.0%, the photocatalytic of Bi_2WO_6 displays the highest degrada-tion efficient. About 98% RhB could be removed in 50 min under visible light irridation. The doped Fe^{3+} is electron deficient, which could act as electron traps and facilitate the separation of photogenerated electron-hole pairs, thus improving the photocatalytic efficiency. Furthermore, the results also reveal that Fe^{3+} doped Bi_2WO_6 nanoarchitecture has high stability and is easy to be recycled.

References:

[1] Fujishima A, Honda K. *Nature*, **1972**,**238**(5358):37-38
[2] Kudo A, Hijii S. *Chem. Lett.*, **1999**,**28**(10):1103-1104
[3] Fu H B, Pan C S, Yao W Q, et al. *J. Phys. Chem. B*, **2005**, **109**(47):22432-22439
[4] Zhu S B, Xu T G, Fu H B, et al. *Environ. Sci. Technol.*, **2007**,**41**(17):6234-6239
[5] Li J P, Zhang X, Ai Z H, et al. *J. Phys. Chem. C*, **2007**,**111** (18):6832-6836
[6] Zhang L S, Wang W Z, Chen Z Q, et al. *J. Mater. Chem.*, **2007**,**17**(24):2526-2532
[7] Li Y Y, Liu J P, Huang X T, et al. *Cryst. Growth Des.*, **2007**,**7**(7):1350-1355
[8] Liu S W, Yu J G. *J. Solid State Chem.*, **2008**,**181**(5):1048-1055
[9] Duan F, Zheng Y, Chen M. *Appl. Surf. Sci.*, **2011**,**257**:1972-1978

[10]Xu J, Wang W, Gao E, et al. *Catal. Commun.*, **2011**,**12**(9):834-838

[11]Shang M, Wang W Z, Zhang L, et al. *Mater. Chem. Phys.*, **2010**,**120**(1):155-159

[12]Shi R, Huang G L, Lin J, et al. *J. Phys. Chem. C*, **2009**,**113**(45):19633-19638

[13]Fu Y, Chang C, Cheng P, et al. *J. Hazard. Mater.*, **2013**, **254-255**:185-192

[14]Wang D J, Zhen Y Z, Xue G L, et al. *J. Mater. Chem. C*, **2013**,**1**(26):4153-4162

[15]Wang D J, Xue G L, Zhen Y Z, et al. *J. Mater. Chem.*, **2012**,**22**(11):4751-4758

[16]Guo S, Li X, Wang H, et al. *J. Colloid Interface Sci.*, **2012**, **369**(1):373-380

[17]Li D F, Guo Y H, Hu C W, et al. *J. Mol. Catal. A*: *Chem.*, **2004**,**207**(2):183-193

[18]Sahel K, Perol N, Chermette H, et al. *Appl. Catal. B*: *Enriron.*, **2007**,**77**(1-2):100-109

[19]Yu T, Tan X, Zhao L, et al. *Chem. Eng. J.*, **2010**,**157**(1):86-92

[20]Fu H, Pan C, Yao W, et al. *J. Phys. Chem. B*, **2005**,**109**(49):22432-22439

[21]Cui Y, Huang J, Fu X, et al. *Catal. Sci. Technol.*, **2012**,**2**(7):1396-140